Natural Resources Research (© 2026)
https://doi.org/10.1007/s11053-026-10739-3

Original Paper

Unconformity-Related Rare Earth Element Mineral Potential of Australia

Arianne Ford,[1,2] Jessica Walsh,[1] Michael Doublier,[1] Antony Burnham,[1] Jonathan Cloutier,[1] Geoff Fraser,[1] Charles Magee,[1] and Karol Czarnota[1]

Received 20 December 2025; accepted 10 June 2026

Heavy rare earth elements (HREE) are critical for the transition to net zero in addition to being key to manufacturing defense technologies. Unconformity-related rare earth element (REE) deposits represent an important source of HREE, including key elements such as dysprosium (Dy) and terbium (Tb). Given the strategic importance of these critical minerals to the national economy, a national-scale mineral potential assessment has been undertaken to evaluate the geological potential for unconformity-related REE mineral systems in Australia. Leveraging previous research into the formation of unconformity-related REE mineral systems in Australia, a new model for the mineral system has been developed based on an existing mineral systems framework. The deposits form as a result of crustal- to deposit-scale processes that operate under favorable spatial and temporal conditions. This study demonstrates how a mineral system that has uncertainties regarding its formation can be used as the basis for predictive modeling through the novel use of datasets not typically utilized in broad-scale mineral potential assessments. Both a knowledge-driven and data-driven approach have been used to generate national-scale mineral potential maps that reduce the exploration search space for unconformity-related REE mineral systems in Australia by up to 95%. In addition to predicting known mineralized regions, the model also demonstrates high prospectivity in parts of Australia where no unconformity-related REE mineralization has previously been identified, particularly on the margins of Precambrian basins in Northern Australia, parts of which remain un- or under-explored.

KEY WORDS: Unconformity-related, Rare earth elements, Critical minerals, Mineral potential mapping, Australia, Resourcing Australia's Prosperity.

INTRODUCTION

Unconformity-related rare earth element (herein referred to as URREE) deposits represent a recently defined type of deposit and could be an important economic and strategic source of heavy rare earth elements (HREE) and yttrium (Y) (Ali et al., 2017; Nazari-Dehkordi et al., 2018; Nazari-Dehkordi & Spandler, 2019; Walsh & Spandler, 2023). The HREE typically include gadolinium (Gd), terbium (Tb), dysprosium (Dy), holmium (Ho), erbium (Er), thulium (Tm), ytterbium (Yb), and lutetium (Lu), and along with yttrium (Y), and represent critical components in the production of high-performance permanent magnets. In particular, Dy and Tb are key to the production of these magnets which are used in the manufacturing of electric vehicles, wind turbines, and solar panels (Liu et al., 2023; International Energy Agency, 2025). Furthermore, the performance and durability

[1]Geoscience Australia, Canberra, Australia.
[2]To whom correspondence should be addressed; e-mail: Arianne.Ford@ga.gov.au

Published online: 27 June 2026

of Dy and Tb at high temperatures make them essential for a range of defense technologies (Goodenough et al., 2018; International Energy Agency, 2025).

It is estimated that over 95% of known rare earth element (REE) resources are directly hosted in or are genetically related to magmatic rocks (and their associated weathering profiles), which has led to global exploration efforts focusing on magmatic mineral systems, such as carbonatites, peralkaline intrusions, and pegmatites (Weng et al., 2015; Spandler et al., 2020; Beard et al., 2023; Ford et al., 2023), and their secondary mineralization processes. However, URREE deposits, which are interpreted to be hydrothermal in origin, represent 12.99% of Australian identified REE mineral resources (Huston et al., 2024) and 7.24% of global resources (Huston, 2024), and are therefore a significant potential source of diversified supply. The Wolverine URREE deposit in the Browns Range region in Western Australia has a total mineral resource estimate (Measured, Indicated, Inferred) of 7.3 Mt @ 0.96% total rare earth oxide (TREO), with a HREO (heavy rare earth oxide)/TREO ratio of 89% (Northern Minerals Limited, 2025). It is difficult to quantify how important URREE deposits are in terms of HREE resources relative to other REE deposit types due to the inconsistent way in which REE resources are reported globally, with most typically just reporting a TREO value.

In addition, it is important to identify opportunities for the production of HREE, whose global supply is currently dominated by China (Weng et al., 2015; Yin and Song, 2022; International Energy Agency, 2025). This concentration poses strategic vulnerabilities for downstream industries reliant on secure and stable access to these critical minerals (Liu et al., 2023; Critical Minerals Office, 2024; International Energy Agency, 2025).

In contrast to most primary REE mineral systems, the mineral system model for the development of URREE deposits is proposed to be low temperature ($T < 300$ °C) and hydrothermal in origin, with no apparent link to syn-mineralization magmatism (Nazari-Dehkordi et al., 2018; Nazari-Dehkordi et al., 2020; Walsh & Spandler, 2023). Globally, there are few known examples of this type of mineral system. The Maw Zone in the Athabasca Basin in Canada is a hydrothermal xenotime deposit that is hosted within brecciated sandstones (Rabiei et al., 2017; Nazari-Dehkordi et al., 2018). In Australia, a number of deposits and occurrences are located across the North Australian Craton, with the most significant mineralization occurring proximal to the Browns Range Dome in Western Australia (Fig. 1; Nazari-Dehkordi et al., 2018). Another occurrence is located at Arthur Popes in the Northern Territory (Fig. 1; Whelan et al., 2023).

Publications on URREE mineralization have typically focused on deposit-scale studies which evaluate detailed microanalytical data to understand potential controls on mineralization (e.g., Nazari-Dehkordi et al., 2018; Walsh & Spandler, 2023; Whelan et al., 2023, and references therein). In this paper, we aim to synthesize these findings to develop a broader formation model using a mineral systems framework that can be applied at a national scale to understand Australia's mineral potential for URREE mineral systems.

Mineral potential mapping using a mineral systems framework can be used to model the physicochemical processes that can lead to the formation of economic mineralization. This typically involves the development of a mineral system model at the relevant scale, translation of conceptual mineral system processes into mappable criteria, data compilation, feature engineering, predictive modeling, validation, and model evaluation (c.f. Ford et al., 2019). The selection of a predictive modeling methodology is dependent on the availability of known mineral deposits and occurrences related to the relevant mineral system formation (Ford et al., 2019). This is critical in the use of data-driven mineral potential modeling which evaluates the relationship between known mineralization and a set of covariates used to represent the mineral system processes. Whereas the use of knowledge-driven methods may be more appropriate if there are insufficient deposits and occurrences with which to train a model, or if other limitations with the training data are observed. Both knowledge- and data-driven models are presented for the URREE mineral system in this study, including discussion of their limitations.

In this study, we present a mineral system model for unconformity-related REEs relevant at the national-scale, followed by a review of available national-scale datasets which can be used to develop mappable criteria, implementation of both knowledge- and data-driven mineral potential mapping methods, and an assessment of the results from both a modeling and geological perspective.

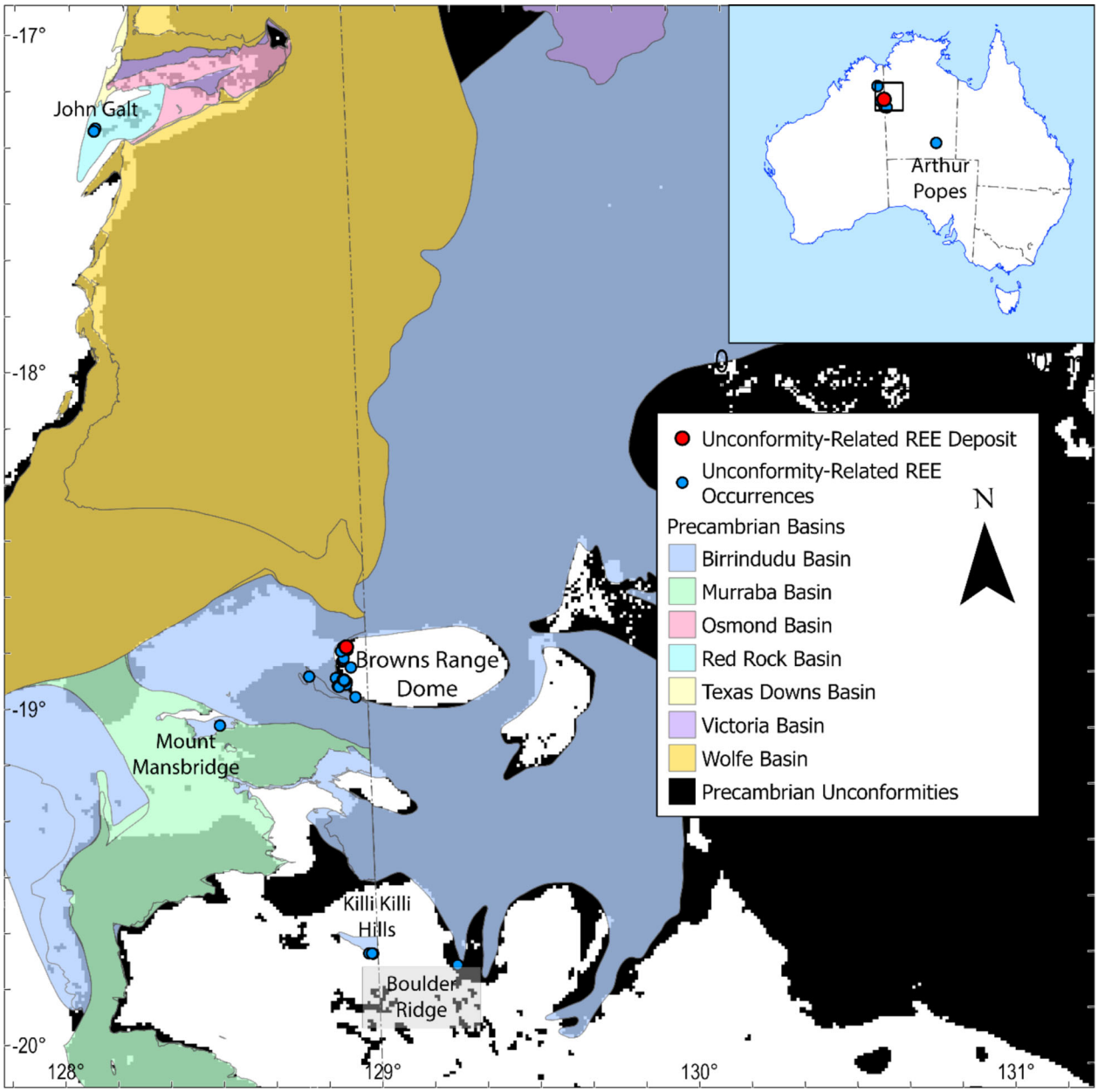

Figure 1. Map of Australian unconformity-related REE deposits and occurrences highlighting the clustering in the Halls Creek–Birrindudu region near the Western Australia-Northern Territory border. Mineral deposit and occurrence data compiled from Nazari-Dehkordi et al. (2018), Department of Mines, Industry Regulation and Safety (2025), and Department of Primary Industry and Resources (2025). Basemap for main image shows Precambrian basins from Raymond (2018) and Precambrian unconformities derived from Vizy et al. (2024).

MINERAL SYSTEM MODEL

Unconformity-related REE deposits are typically enriched in HREE such as Dy and Tb (Nazari-Dehkordi et al., 2018; Spandler et al., 2020; Walsh & Spandler, 2023). The mineralization is hydrothermal in origin, structurally controlled, and typically occurs as xenotime with some florencite (Nazari-Dehkordi et al., 2018; Nazari-Dehkordi and Spandler, 2019). Based on examples in the Athabasca Basin in Canada (e.g., Maw Zone; Rabiei et al., 2017), and in northern Australia (e.g., Western Tanami region

and Halls Creek Orogen), there appears to be no genetic link to syn-mineralization magmatism (Nazari-Dehkordi et al., 2017; Nazari-Dehkordi et al., 2018).

Although showing some similarities to unconformity-related uranium mineral systems, key differences relate to the apparent lack of redox control on the URREE precipitation, as HREE + Y solubility in hydrothermal fluids is unlikely to be strongly affected by redox reactions (Nazari-Dehkordi et al., 2018). In addition, the mineralogy of the URREE deposits (xenotime-dominant) differs to that of typical uraninite-dominant unconformity-related uranium systems (Bruce et al., 2020). As such, Australian unconformity-related uranium deposits and occurrences have not been considered in building the URREE mineral system model presented here.

Using the example of Browns Range (western Tanami region; e.g., Nazari-Dehkordi et al., 2018) and John Galt (Halls Creek Orogen; e.g., Walsh & Spandler, 2023) in Northern Australia (Fig. 1), a generalized mineral system model has been developed for the Australian context using the framework of Skirrow et al. (2019). The framework incorporates four mineral system components: (1) sources of metals, fluids, and ligands; (2) energy sources and fluid flow drivers; (3) fluid flow pathways and lithospheric architecture; and (4) ore depositional gradients or traps.

The simplified deposit formation model (Fig. 2) involves fluid mixing between (1) saline HREE + Y-bearing fluids from underlying basement rocks and (2) low-pH phosphorus (P)-bearing fluids derived from the overlying basin (Nazari-Dehkordi et al., 2019), at or near the unconformity between basement (e.g., Browns Range Metamorphics) and basin (e.g., Birrindudu Basin), where both fluids are transported along faults. The REE in the fluids are leached from radiation-damaged zircons, with ore formation (i.e., precipitation of xenotime with minor florencite) estimated to have occurred at (hydrothermal) temperatures between 150 and 300 °C (Nazari-Dehkordi et al., 2018; Spandler et al., 2020). It is also noted by Nazari-Dehkordi et al. (2018) that carbonate minerals appear to be completely absent in the mineral assemblage. An alternative to the two-fluid mixing model has been proposed and suggests that the REE and P required for the xenotime (and minor florencite) mineralization were derived from the same source, this being the Browns Range Metamorphics zircon. It is possible that the REE and P could have been transported in low-pH saline fluids as $REECl^{2+}$ or $REECl_2^{+}$ and $H_2(PO_4)^{-}$, respectively (Gysi et al., 2015; Migdisov et al., 2016; Walsh & Spandler, 2023).

Timing of the URREE mineralization in northern Australia (1.65–1.61 Ga; Morin-Ka et al., 2016; Nazari-Dehkordi et al., 2020) coincides with abrupt changes in the apparent polar wander path, which has been attributed to major continental collision events involving the North Australian Craton, with the timing of mineralization coinciding with the Isan and Liebig orogenies (Spandler et al., 2020). Notably, the timing of mineralization does not correspond to any currently identified magmatic or orogenic event in the Browns Range region.

It has been demonstrated that the basement metasedimentary rocks (i.e., Browns Range Metamorphics) are the source of REE (Nazari-Dehkordi et al., 2017), and further that the zircon derived from these rocks hosted the majority of the HREE inventory which was mobilized and concentrated to form the orebodies (Walsh & Spandler, 2023). As such, zircon from the basement metasedimentary rocks has been demonstrated to be the source in URREE deposits at Browns Range (western Tanami region) and John Galt (Halls Creek Orogen). These zircons are derived from a Mesoarchean granitic source and were subject to radiation damage and metamictization between ca. 3.1 and 2.6 Ga, i.e., 500 my. in duration. Weathering and erosion of the granitic source during the late Archean led to deposition of the basement metasedimentary rocks (i.e., Browns Range Metamorphics) and was the likely the timing of uptake of 'non-formula' elements (REE, Y, U, Th, Nb, P, Al, Ca, Fe, Ti, F, OH^{-}, and/or H_2O) into the metamict zircon (Walsh & Spandler, 2023). Important to the mineral system model, metamictization was sustained due to a lack of thermal annealing across the Late Archean into the Paleoproterozoic. Therefore, sustained tectonic quiescence or conditions which prevent the radiation-damaged zircon from annealing are considered important (Walsh & Spandler, 2023). Laboratory testing suggests that recovery of partially radiation-damaged zircon starts as low as 400–500 °C and progresses to approximately 1400 °C (Magee et al., 2025). Pervasive circulation of saline basinal brines at ca. 1.65–1.61 Ga allowed leaching of REE (and possibly P) from the metamict zircons (Walsh & Spandler, 2023). Migration of these fluids into fault zones or along the overlying unconformity led to the two fluids mixing and the subsequent crystallization

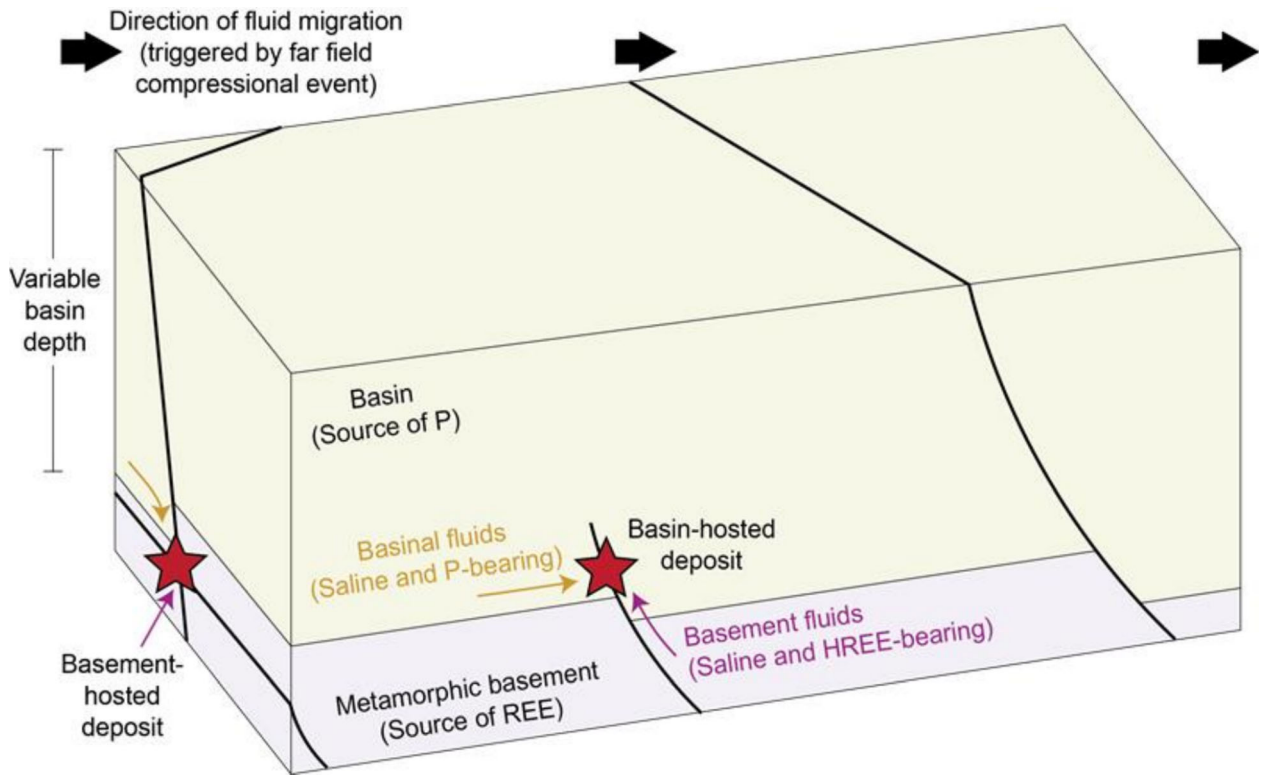

Figure 2. Simplified formation model for unconformity-related REE deposits. Based on the models of Nazari-Dehkordi et al. (2018) and Rabiei et al. (2017).

of the xenotime (and minor florencite) resulting in mineralization (Walsh & Spandler, 2023). Nazari-Dehkordi et al. (2018) note that the xenotime which hosts the REE mineralization contains anomalous U and Th.

Most Australian URREE deposits are distributed along the edges of the thick Kimberley Craton which has been stable since the Mesoarchean and can be mapped by the depth to the lithosphere-asthenosphere boundary (LAB; Hoggard et al., 2020; Sudholz et al., 2023). Through time, the craton would be an ideal source of saline fluids as low-elevation platforms enhance evaporite formation and could shield basins developed along the cratonic edge from excessive subsequent deformation typically localized along thinner portions of the lithosphere (Czarnota et al., 2020).

It is noted that although previous work has suggested a possible URREE occurrence at Korella in northwest Queensland (Jaireth et al., 2014; Spandler et al., 2020), a more recent publication attributes the occurrence as sedimentary REE-enriched phosphorite (Valetich et al., 2022; Huston et al., 2024), leading to its exclusion from this mineral potential assessment.

DATA

The mineral potential assessment in this study incorporates multidisciplinary precompetitive geoscience data from 21 unique datasets published by Geoscience Australia, and Australia's state and territory geological survey organizations. Table 1 shows the datasets used to develop the 12 mappable criteria used as spatial proxies for the relevant mineral systems processes related to the formation of URREE deposits in Australia.

Currently, no national-scale map of regional-scale unconformities has been published for Australia. In order to generate this critical input for the URREE mineral potential assessment, we utilized published 3D chronostratigraphic surfaces of Australia and their associated isochores (Vizy et al., 2024). By extracting areas from the isochores where younger surfaces overlie older surfaces and con-

Table 1. Mappable criteria and datasets used in the (Precambrian) unconformity-related REE mineral potential assessment for Australia, including associated subjective map weightings and thresholds

Mineral system component	Mappable criterion	Dataset reference	Weightings				Thresholds
			Importance	Applicability	Confidence	Map weight	
Sources of metals, fluids, and ligands	Distance to Precambrian metamorphic units	Geoscience Australia and Australian Stratigraphy Commission (2025), Sanchez et al. (2024)	0.900	0.800	0.800	0.576	20 km
	Distance to Precambrian basins	Raymond (2018), Geological Survey of Western Australia (2022)	0.900	0.900	0.900	0.729	50 km
	Distance to zircons exhibiting characteristics that may be indicative of radiation damage	Geoscience Australia (2025)	0.900	0.700	0.700	0.441	50 km
Energy sources and fluid flow drivers	Distance to Precambrian orogenic events	Raymond (2018)	0.800	0.500	0.800	0.320	200 km
	Distance to major crustal boundaries	Doublier and Korsch (2024)	0.800	0.500	0.900	0.360	100 km
Fluid flow pathways and lithospheric architecture	Distance to Precambrian unconformities	Vizy et al. (2024)	1.000	0.800	0.800	0.640	20 km
	Distance to faults	Colquhoun et al. (2025), Department of Energy, Environment and Climate Action (2025), Department of Natural Resources and Mines, Manufacturing, and Regional and Rural Development (2025), Geological Survey of South Australia (2025a, 2025b, 2025c, 2025d), Geological Survey of Western Australia (2025), Mineral Resources Tasmania (2025), Northern Territory Geological Survey (2023), Northern Territory Geological Survey and Geognostics Australia Pty Ltd. (2021), Sanchez et al. (2024)	1.000	0.900	0.800	0.720	20 km
	Distance to 185 km contour of lithosphere-asthenosphere boundary (LAB)	Hoggard et al. (2020)	0.800	0.700	0.700	0.392	100 km
Ore depositional gradients (traps)	HREE + Y catchment anomalies	de Caritat and Cooper (2011)*	0.900	0.700	0.600	0.378	400 ppm HREE + Y
	Xenotime (+/- Florencite) anomalies in catchments	de Caritat et al. (2023)*	0.900	0.700	0.600	0.378	0.0015 ratio (xenotime + florencite)/total count
	Lack of carbonate minerals in catchments	de Caritat et al. (2023) *	0.700	0.600	0.600	0.252	0.00001 ratio carbonates/total count

Table 1. continued

Mineral system component	Mappable criterion	Dataset reference	Weightings				Thresholds
			Importance	Applicability	Confidence	Map weight	
U and Th radiometric anomalies	Wilford and Kroll (2020)	0.700	0.700	0.700	0.343	5 km to coincident U (>1 ppm) and Th (>10 ppm) anomaly	

The weightings for importance (I), applicability (A), and confidence (C) are multiplied to get the overall map weight (W). Further information on the development of the mappable criteria is included in the assessment criteria table in the data package for this model, provided in the Data Availability section

*Indicates dataset has incomplete national coverage and imputation has been used to fill data gaps

straining the isochores to those available from the Precambrian (Neoproterozoic-Mesoproterozoic, Neoproterozoic-Neoarchean, and Mesoproterozoic-Neoarchean), we were able to generate a map of regional unconformities of Australia (Fig. 3a). Vizy et al. (2024) also publish data uncertainty maps that can be considered when assessing the associated 3D chronostratigraphic surfaces used to generate the isochores due to the variable data coverage available at the national-scale. Although nominally generated for use in national groundwater assessments, the 3D chronostratigraphic surfaces demonstrate that non-traditional geoscience datasets from other fields can be effectively utilized for mineral exploration studies.

A review of all available zircon spot analysis data from Geoscience Australia's Sensitive High Resolution Ion Microprobe (SHRIMP) indicates that very few zircons are attributed as metamict (Geoscience Australia, 2025). As the spot analyses are undertaken for the purposes of SHRIMP age dating, metamict zircons are typically avoided prior to or during analysis. This is because the same open system behavior that allows REE mobilization (and the formation URREE deposits) also results in the loss of radiogenic Pb from the zircon. As the two uranium isotopes decay at different rates, Pb loss causes discordance between the ages derived from the $^{206}Pb/^{238}U$ and $^{207}Pb/^{235}U$ isotopic systems. This allows radiometric age discordance to be used as a direct measure of zircon metamictization and trace element open system behavior. If metamictization is pervasive enough in the zircon population of a rock, then the SHRIMP analyst will be unable to avoid analyzing metamict grains with every individual spot analysis. By extracting analyses with an age ≥ 1000 Ma, $\geq 20\%$ discordance, and > 50 ppm U, regions that have potentially been subject to an extended period of time in the uppermost crust at lower temperatures than the zircon annealing temperature (e.g., Ewing et al., 2003) have been identified (Fig. 3b).

While it is acknowledged that some parts of Australia remain under sampled for zircons, most outcropping areas are relatively well sampled. The distribution of the zircon samples also raises the question of evidence of absence vs. absence of evidence. Unlike the National Geochemical Survey of Australia (NGSA; de Caritat and Cooper, 2011), and Heavy Mineral Map of Australia (HMMA; de Caritat et al., 2023) datasets which are clear examples of evidence of absence due to a documented

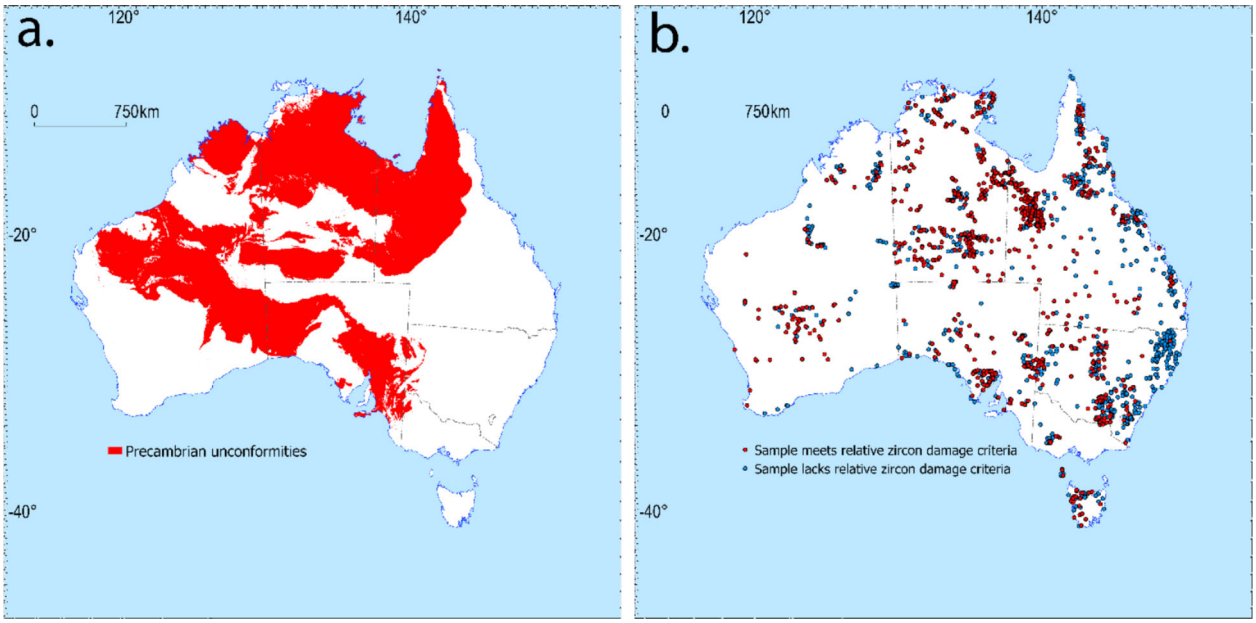

Figure 3. (**a**) Map of Precambrian unconformities derived from published 3D chronostratigraphic surfaces and their associated isochores (Vizy et al., 2024) and (**b**) map of individual zircon spot analyses from Geoscience Australia's SHRIMP (Geoscience Australia, 2025) indicating which analyses demonstrate an age ≥ 1000 Ma, ≥ 20% discordance, and > 50 ppm U, used as a proxy for relative zircon damage (metamictization).

lack of sampling in some areas, with the zircon data, it remains unclear as to whether an area has not been sampled, or if it is simply that no zircons were identified in samples (i.e., absence of evidence). For the purposes of this model, this dataset is assumed to have full national coverage, acknowledging this limitation.

It is noted that the maps generated from the NGSA and HMMA datasets contain incomplete national coverage. In particular, samples are not currently available in parts of Western Australia and the Northern Territory, which includes the region where most of the currently identified deposits and occurrences are located. In order to account for this region of missing data in the modeling process, imputation has been used to assign a probability score of 0.5 to these areas so as to not excessively downgrade their prospectivity due to lack of data (c.f. Ford et al., 2023). This value of 0.5 represents the classification threshold between more prospective and more unprospective areas, as it represents a mid-point value where the prospectivity cannot be determined either way due to lack of data in the specified dataset.

MINERAL POTENTIAL MAPPING

At the national-scale in Australia, the focus of mineral potential mapping is not to identify individual mineral deposits, but to model the broad-scale processes that can lead to the formation of mineral systems. A knowledge-driven weighted sum approach has been implemented here based on the sparsity of known mineral deposits and occurrences.

Although 33 known URREE deposits and occurrences have been identified in Australia, due to their extremely high degree of clustering over a relatively small area, they really only represent six distinct mineralized areas (Fig. 1). Furthermore, when the 1 km cell size of the model is considered, the clustering means that only 24 model cells contain a URREE deposit or occurrence. Duplicates were removed for the purposes of the mineral potential assessment, resulting in 24 positive labels being available to train, test, and validate a data-driven model such that only $\sim 0.0003\%$ of the model's feature vectors contain a positive training label. This limitation on availability of suitable training data, combined with the lack of data coverage over the area containing 22 of the 24 known deposits and occurrences in the NGSA and HMMA datasets, and the limited examples used to develop an under-

standing of the broad-scale processes involved in the formation of the mineral system, led to the implementation of a knowledge-driven model which can factor in these limitations. A random forest machine learning model has also been generated for comparison purposes, although it is not considered robust.

In order to facilitate the meaningful integration of the different input maps, each input was first normalized to a [0, 1] scale to account for the different units used in the underpinning datasets. Table 1 outlines the thresholds and weightings applied to each input map for the knowledge-driven model based on the certainty definitions of Meyer and Brooker (1991). The mid-point value of 0.5 was assigned to the threshold for each map.

Thresholds for each input map into the knowledge-driven model were assigned based on the understanding of the constituent mineral system processes. For example, setting a threshold at 20 km from Precambrian metamorphic units means that raster cells at 20 km from these units are assigned a value of 0.5, with closer cells assigned higher values, and more distal cells assigned lower values. The thresholds guide how quickly prospectivity drops off away from the feature of interest in the model.

Each input map was then assigned an importance, applicability, and confidence weighting on a [0, 1] scale. The importance value represents the overall importance of the criterion to the formation of the mineral system, the applicability represents a measure of how well the map characterizes the mineral system process that it is a spatial proxy for, and the confidence reflects the quality of the data source used to generate the map in terms of spatial coverage, accuracy, and general data quality (e.g., Skirrow et al., 2019; Ford et al., 2023). These three weighting factors were then multiplied together to assign an overall weight for each input map for the knowledge-driven model.

While typically all mineral system components would be assigned an equal weighting factor in the integration stage, in the URREE mineral system, it is acknowledged that the drivers of the fluid flow can occur distally to the local mineralizing event. As hypothesized by Nazari-Dehkordi et al. (2018), the far field orogenic and collisional events that are interpreted to have triggered fluid circulation at Browns Range potentially occurred over 1000 km away. This essentially means that any part of the Australian continent during the Precambrian could be considered favorable in terms of fluid flow drivers. While the triggering events must have occurred, their spatial proximity in this case is less important. As such, the weighting assigned to each mineral system component has been varied in order to reduce the importance of the energy sources and fluid flow drivers in the knowledge-driven model (Table 2).

The weighted input maps were then combined using a weighted sum approach (Fig. 4) that factors in the component weights to generate the final mineral potential model (c.f. Skirrow et al., 2019; Ford et al., 2023). Figure 5 shows the knowledge-driven mineral potential model and associated data availability map.

The success-rate curve (Fig. 6), area-under-the-curve (AUC = 0.998), and F_1-score (F_1 = 0.727)

Table 2. Component weights (subjective) used in the unconformity-related REE mineral potential assessment for Australia.

Mappable criterion	Mineral system component	Component weight
Distance to Precambrian metamorphic units	Source of metals, fluids, and ligands	0.3
Distance to Precambrian basins		
Distance to zircons exhibiting characteristics that may be indicative of radiation damage		
Distance to Precambrian orogenic events	Energy sources and fluid flow drivers	0.1
Distance to major crustal boundaries		
Distance to Precambrian unconformities	Fluid flow pathways and lithospheric architecture	0.4
Distance to faults		
Distance to 185 km LAB contour		
HREE + Y catchment anomalies	Ore depositional gradients or traps	0.2
Xenotime (+/− Florencite) anomalies in catchments		
Lack of carbonate minerals in catchments		
U and Th radiometric anomalies		

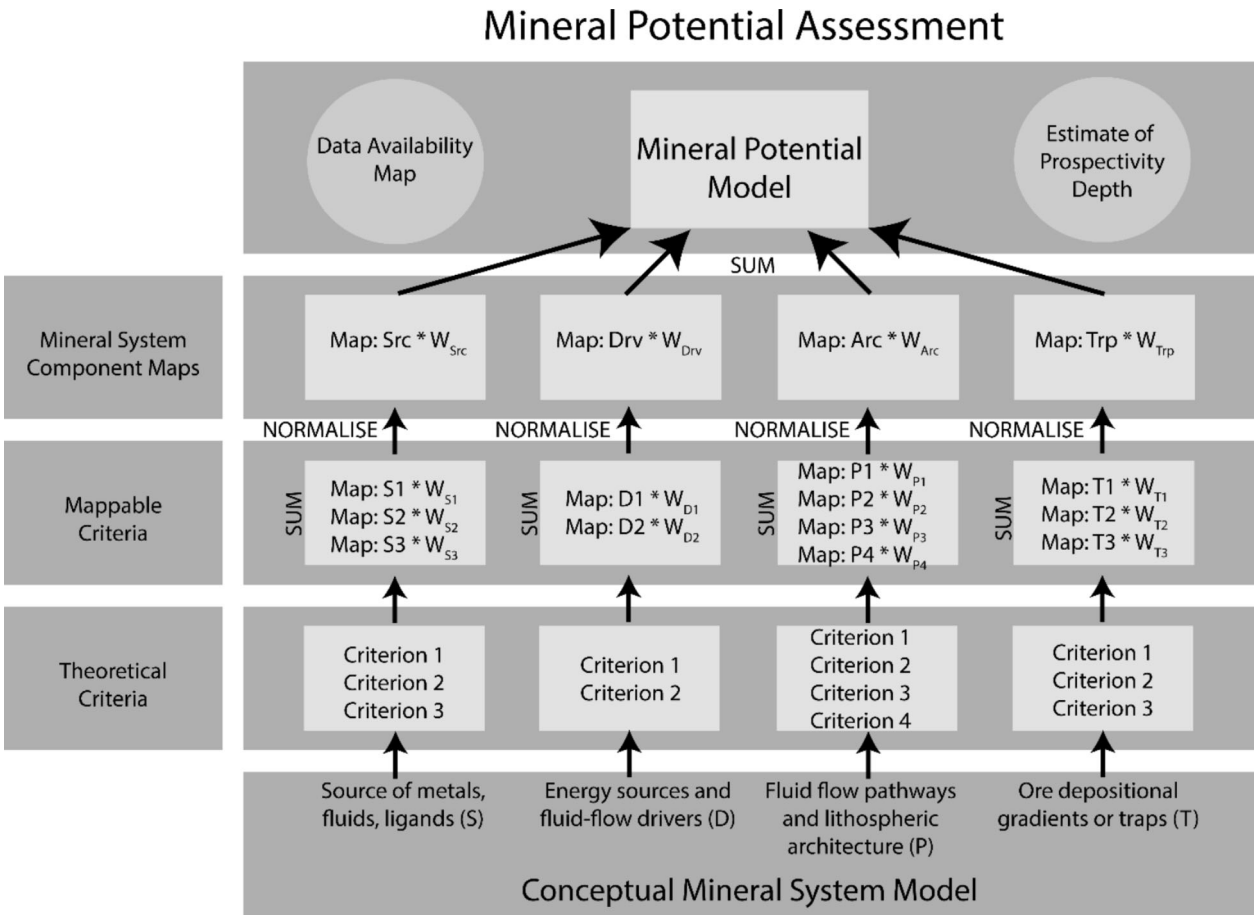

Figure 4. Workflow for mineral potential assessment using knowledge-driven weighted sum methodology (modified after Skirrow et al., 2019).

were evaluated as validation metrics for the knowledge-driven model in Figure 5a (c.f. Nykänen et al., 2023). The AUC metric represents the probability that the model, if given randomly selected positive and negative labels, will show higher prospectivity for the positive label than the negative label (e.g., Lawley et al., 2022; Ford et al., 2023). The F_1-score is the mean of the precision, and recall which considers true positives, and both false positives and false negatives (e.g., Parsa and Cumani, 2025). The F_1-score calculations assign model values ≥ 0.5 as prospective, and model values < 0.5 as unprospective. The mean F_1-score was evaluated from 10 iterations that utilize all of the positive labels and 10 draws of 24 random locations used as negative labels.

Due to the incomplete data coverage for the input maps derived from the NGSA and HMMA datasets, a ''full coverage'' model was subsequently generated which only included input maps with complete national data coverage. The full coverage model and its corresponding success-rate curve are shown in Figure 7a and b, respectively. The model in Figure 7a produces an AUC of 0.960 and an F_1-score of 0.739.

A random forest model (e.g., Rodriguez-Galiano et al., 2014) was generated for comparison purposes using a 5-fold cross-validation approach, despite the limitations of the training data, and some of the input datasets discussed in the Data section. The 24 URREE deposits and occurrences that had been filtered to remove duplicates in each cell were split approximately 60-20-20 (15-4-5) for

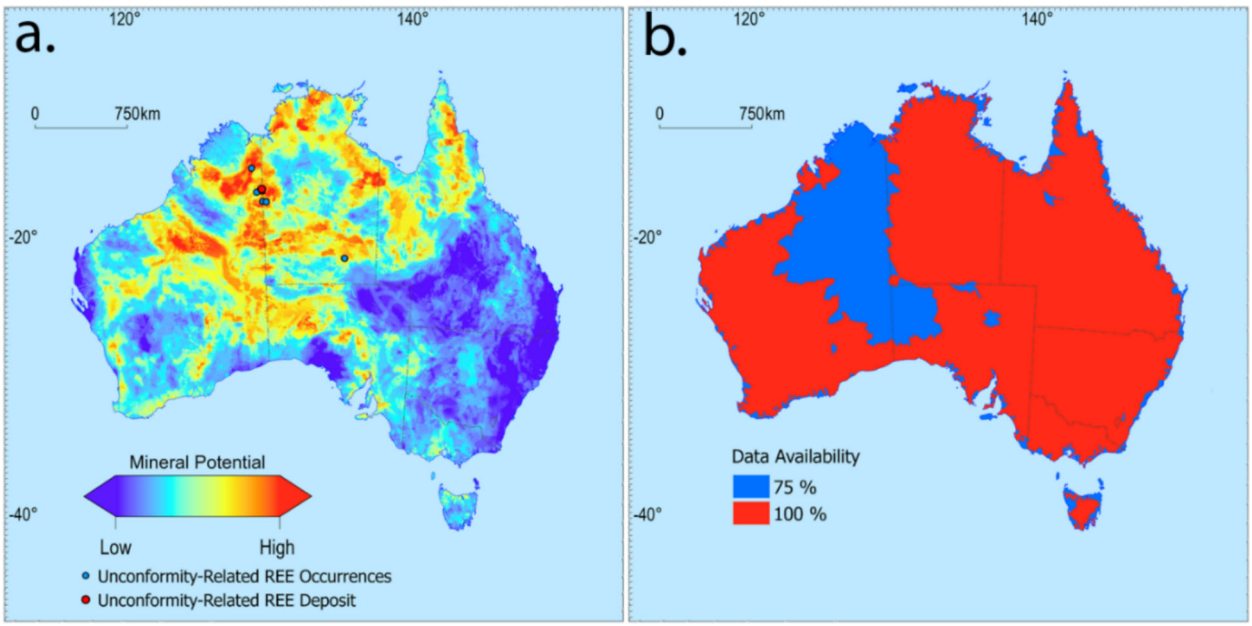

Figure 5. **a** Knowledge-driven mineral potential map using all input maps and **b** corresponding data availability map for URREE mineral systems in Australia.

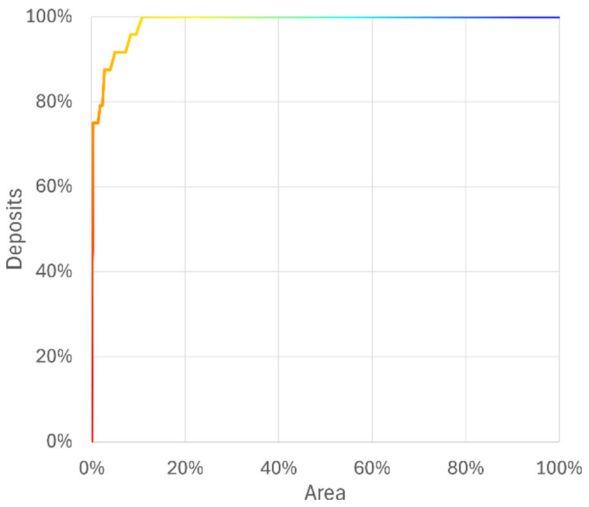

Figure 6. Success-rate curve for the URREE mineral potential model in Figure 5a. The color ramp used in the plot matches the colors in the mineral potential model.

training, testing, and validation purposes, respectively, with the tree depth set to 7, and the number of trees set to 101. Negative labels were randomly generated in feature vectors that did not contain a positive label, with the number of negative labels set to equal the number of positive labels used for training and testing to avoid unbalanced labels. Figure 8a shows the mineral potential model produced using a random forest machine learning model. The corresponding success-rate curve is shown in Figure 8b, and Figure 9 shows the mean absolute Shapley (SHAP) values which quantify the influence of each individual input map on the model (e.g., Parsa et al., 2024). Area-under-the-curve (AUC = 1.000) and F_1-score (F_1 = 1.000) were evaluated as validation metrics for the random forest model using the five validation positive labels.

For the purposes of evaluation, the negative labels used in both the AUC and F_1-score calculations are randomly generated locations that do not intersect model pixels that contain known deposits and occurrences, and the positive labels are the 24 deposits and occurrences that are not duplicates within the model cells. As the positive labels are subset for training, testing, and validation of the random forest model, only five negative labels were generated for validation of this model to be equivalent to the number of positive hold-out labels available for validation.

DISCUSSION

Due to the limited number of currently identified URREE deposits and occurrences in Australia,

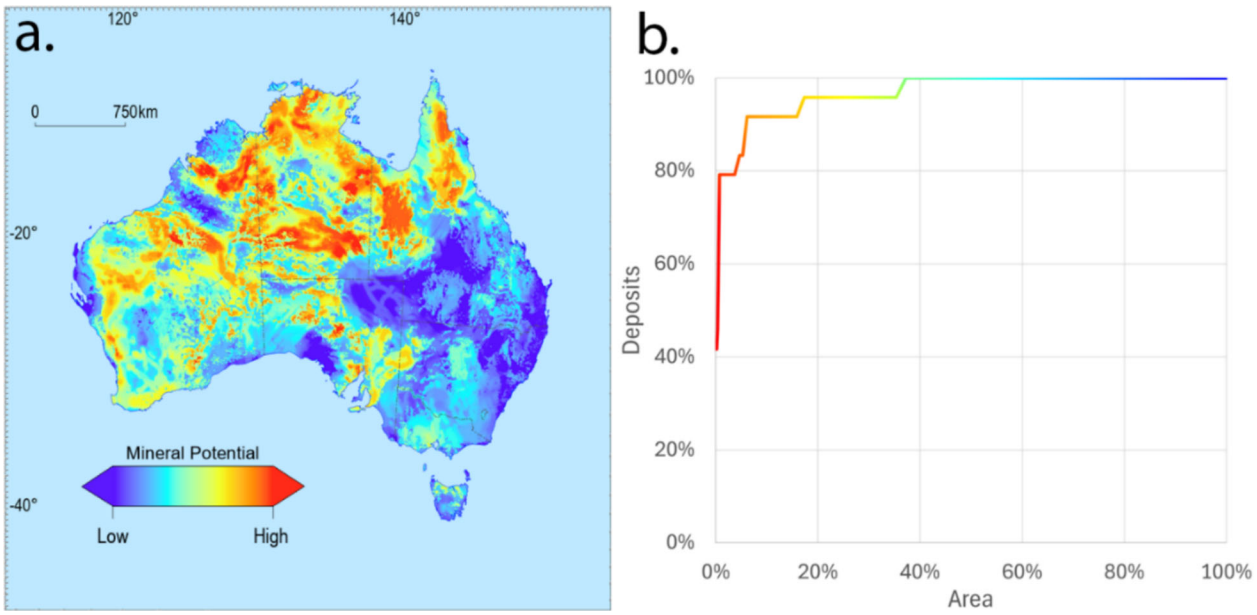

Figure 7. (**a**) Knowledge-driven mineral potential map using the nine input maps with full national data coverage and (**b**) corresponding success-rate curve for the mineral potential model in (**a**). The color ramp used in the plot matches the colors in the mineral potential model.

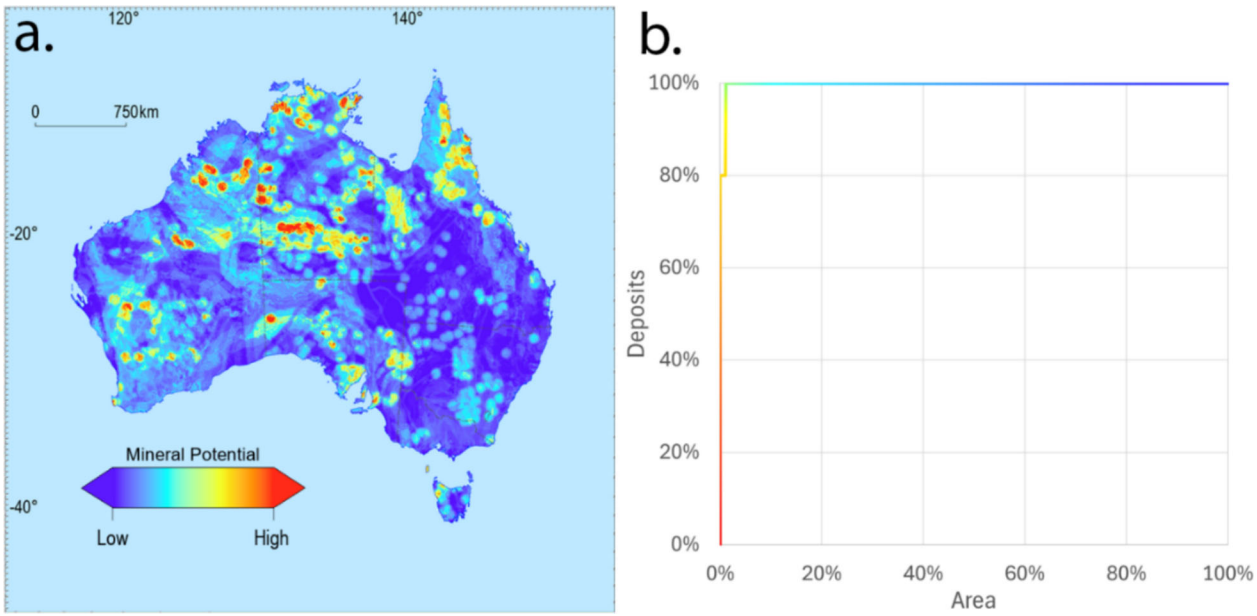

Figure 8. (**a**) Random forest-based mineral potential model and (**b**) success-rate curve with the color ramp matching the mineral potential model in (**a**).

combined with their highly clustered spatial distribution (Fig. 1), a knowledge-driven weighted sum approach was utilized to generate a national-scale mineral potential model. Weighting factors relating to the importance, applicability, and confidence of each input map, and the relative contribution of each mineral system component, have been subjectively assigned by the authors based on the com-

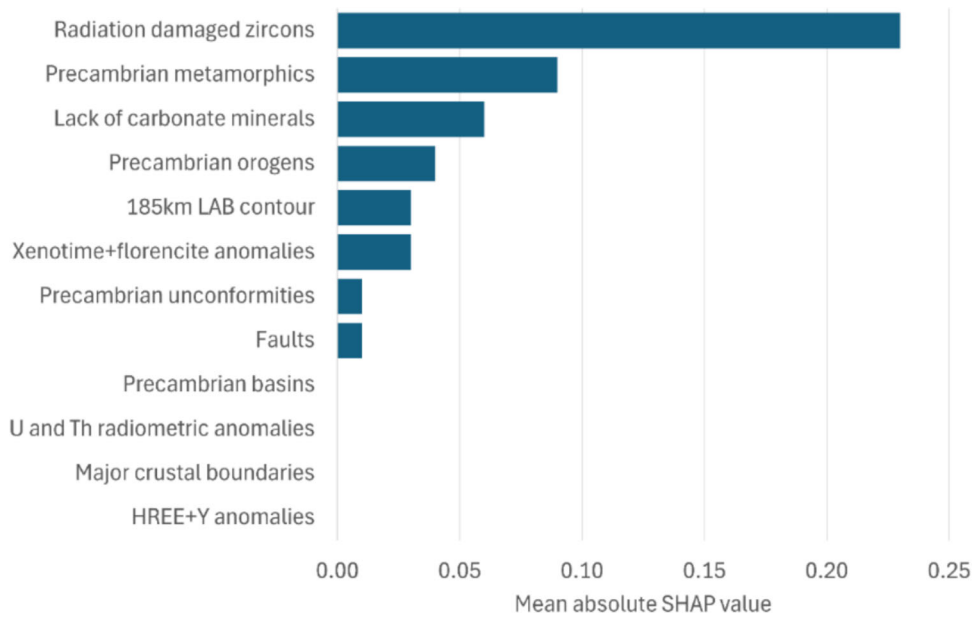

Figure 9. Mean absolute SHAP contributions (influence on model output) for the random forest model in Figure 8a.

bined understanding of the mineral system, and the fundamental underpinning datasets used in the assessment.

Where appropriate and possible, the input maps for the mineral potential models were constrained to the Precambrian (Table 1), as the source, host, and timing of mineralization (and constituent processes) of URREE mineral systems in Australia are associated with Precambrian basement, and unconformably overlying Proterozoic basin material. A comprehensive understanding of thermal history is important to this mineral system model. Specifically, long-term, possibly up to 500 million years (Ewing et al., 2003; Walsh & Spandler, 2023), tectonic quiescence is required for zircon to be subject to radiation damage and metamictization, followed by mobilization of non-formula elements which provided the ingredients for ore formation.

In order to evaluate the knowledge-driven mineral potential maps in Figures 5a and 7a, a success-rate curve was plotted, and AUC and F_1-score values calculated using the location of the 24 identified URREE deposits and occurrences as positive labels, and 24 random locations as negative labels, as these were not used to train the model. The knowledge-driven mineral potential model in Figure 5a produces an AUC of 0.998 and predicts 91.7% of the URREE deposits and occurrences within 5.0% of the area, reducing the exploration search space by approximately 95% (Fig. 6). A mean F_1-score of 0.727 was obtained for the model and evaluated from 10 iterations that utilize all of the positive labels and 10 draws of 24 random locations used as negative labels.

The full coverage knowledge-driven mineral potential model in Figure 7a, which excludes the input maps derived from the NGSA and HMMA datasets that do not have full national data coverage, predicts 91.7% of the URREE deposits and occurrences within 6.1% of the area. This model produces an AUC of 0.960 and an F_1-score of 0.739. In comparison with the model containing all 12 input maps in Figure 5a, a slightly weaker AUC value was obtained; however, the F_1-score was slightly better for the full coverage model in Figure 7a; however, the full coverage model may be considered more robust. Arguably, both models are important, as understanding the impact of incomplete data helps support decision making around future data acquisition programs.

The relatively high AUC values yet moderate F_1-scores obtained for both the knowledge-driven models suggest that both models are good at distinguishing between the positive and negative (random) labels; however, they appear to perform less effectively when the assigned prospective/un-

prospective threshold is 0.5. While in some cases, this disparity between the AUC value and F_1-score can be caused by imbalanced datasets, this study pre-emptively mitigates the issue by intentionally setting the number of negative labels to be equal to the number of positive labels to avoid the imbalance in the first place. Modifying the classification threshold to 0.9 resulted in mean F_1-scores of 0.884 and 0.957 for the weighted sum model with all input maps and the full coverage model, respectively, both notable improvements over the default classification threshold. While this revision of the classification threshold clearly improves the F_1-score metrics, a question remains as to whether the change is reasonable given the approach to feature engineering in general, and more specifically, the imputation value assigned to fill in data gaps for 3 of the 12 input maps for the model in Figure 5a, which assigns a value of 0.5 as the threshold between prospective and unprospective.

Despite the limited number and clustering of known URREE deposits and occurrences, a random forest machine learning model was generated for comparison using all 12 input maps. The model in Figure 8a predicts 100% of the five URREE validation points within 1.1% of the area, thus reducing the exploration search space by approximately 98.9% (Fig. 8b). A perfect AUC value of 1.000 and a mean F_1-score of 1.000 were obtained for the model.

Although the validation metrics produced by the random forest model are clearly exceptional, the limitations relating to the number of known deposits and occurrences with which to train and test any machine learning model, and their very high degree of clustering, bring the robustness of the random forest model results into question. This is demonstrated by the perfect AUC and F_1-score values obtained which are indicative of the model overfitting. Although 24 positive labeled points were available, the approximately 60-20-20 (15-4-5) train-test-validation split meant that the model was typically selecting only $\sim$ 4 positive labels as test points and only 5 were used as hold-out validation points. Their clustering also compounds this issue, as the test and validation points come from the same clusters as the training points, and are thus not entirely independent. While approaches exist to ensure that training and validation points are not drawn from the same clusters, such approaches assume sufficient numbers of labeled data exist to effectively sample each cluster—assumptions which do not hold in this case study.

Methods for augmentation of the training data to address this were considered, but ultimately not implemented by the authors due to weaknesses in the algorithms predominantly as a result of the spatial biases in the original positive labels dataset which would propagate (e.g., limited samples, spatial clustering). As the models being developed are intended to support a broad spectrum of applications—including mineral exploration, government planning and policy, infrastructure development, investment decisions, and community engagement—it was important to prioritize input reliability and reduce the introduction of additional uncertainty. While augmented or synthetic training data offer promising avenues for improving model performance, their inclusion presents challenges for validation, often requiring substantial exploration efforts such as sampling, geophysical surveys, or drilling to ensure confidence in their accuracy. Choi et al. (2025) discuss similar limitations with regards to confidence in the generation of synthetic or augmented labels to overcome the scarcity of sufficient training data in seismic interpretation.

The predictive importance of the input maps was evaluated from calculating SHAP values (e.g., Parsa et al., 2024). Figure 9 shows the mean absolute SHAP values for the mineral potential model as shown in Figure 8a. Notably, the SHAP values demonstrate that the input maps derived from the NGSA and HMMA datasets perform relatively poorly. This is almost certainly due to the fact that the majority of the positive labels used to train and test the model are located in an area of missing data where imputed values were used. Precambrian unconformities also perform relatively poorly according to the SHAP values obtained, which is an unexpected result given the mineral system being modeled and all of the positive labels being located proximal to or within the mapped Precambrian unconformities. It is unclear why this conceptually important map appears to contribute so little to the model output, but may potentially be impacted by multiple factors, including: (1) an inability to differentiate between the positive and negative labels, though multiple model runs demonstrate similar results, and/or (2) a result of insufficient training and test labels as previously noted.

A comparison of the subjectively assigned overall weights (Table 1) with the SHAP values derived from the random forest model (Fig. 9) demonstrates no relationship. While for some maps, this may be especially attributed to the subjective

applicability and confidence weights, for other maps, there remains no clear explanation for the divergence.

The national-scale mineral potential models in Figures 5a and 7a show elevated prospectivity in regions with known URREE mineralization, such as the Halls Creek-Birrindudu region on the Western Australia-Northern Territory border, and around Arthur Popes in the Northern Territory (Fig. 10).

In addition, the models highlight high prospectivity in parts of the Yeneena, Officer, Bentley, Osmond, Louisa, and Murraba basins in Western Australia; parts of the Amadeus, Ngalia, South Nicholson, Georgina, and McArthur basins in the Northern Territory; the Mount Isa region in Northwest Queensland, and parts of Northeast Queensland relating to the Etheridge and Savannah sedimentary provinces; and finally, parts of the Cariewerloo Basin in South Australia (Fig. 10). It is interesting to note that not all Precambrian basins demonstrate high prospectivity (e.g., Hamersley, Ashburton, Earaheedy, Edmund, and Kimberley basins in Western Australia). Review of the modeling inputs indicates that these relatively unprospective Precambrian basins typically lack mapped Precambrian metamorphics, and fewer and/or less extensive U and Th anomalies in the radiometric data. They also correspond to areas that lack geochemical or mineralogical anomalies relevant to the mineral system from the NGSA and HMMA datasets respectively, despite being in areas with complete data coverage (Fig. 5b).

Although not included as an input to the model presented here, it has been noted by the authors that the URREE mineralization in the Browns Range region appears to have a close spatial association with Precambrian glauconitic rocks in both surface and interpreted bedrock geology (Raymond et al., 2012; Sanchez et al., 2024). At this time, it is unclear what process in their formation would relate to the development of an URREE mineral system other than simply being an indication that an unconformity may exist nearby. This is a spatial association that warrants further investigation in the future to ascertain whether a specific causal relationship between glauconites and URREE mineral systems exists.

The mineral potential assessment has demonstrated that despite some challenges relating to data availability and coverage, novel methods for mapping spatial proxies for key mineral systems processes can be applied. In particular, we have developed a consistent way to map regional unconformities at the national scale in Australia (Fig. 3a), and how individual zircon spot analyses can be used to identify regions that may be more prone to zircon damage (metamictization) which allows the REE to be leached and form a deposit (Fig. 3b).

MODEL LIMITATIONS

The quality of any mineral potential model is contingent on the quality of the fundamental datasets used to generate the input maps. While all reasonable effort has been made to ensure the quality of the input datasets, there remain some limitations. In particular, it is noted that the maps of distance to Precambrian basins and distance to Precambrian unconformities are both derived in full, or in part, from basins extracted from Raymond (2018). Due to the complexity of mapping Precambrian basins which may have undergone extensive subsequent deformation and/or metamorphism, it is acknowledged that some of these strongly deformed basins may be missing from the analysis. Further to this, their extents may not be well constrained due to erosion which may mean the maximum extent in their geological evolution is not well represented, and/or constraints are limited in areas with less geological data or understanding.

It is acknowledged that some spatial correlation exists between some of the datasets used to represent different mineral system components in the modeling. This is not unexpected due to the interrelationship between processes which are not independent. Figure 11 shows the correlation matrix for the 12 input maps used in the knowledge-driven and random forest models (Figs. 5a and 8a). The only notable correlations (≥ 0.5) exist between the unconformities and basins, and the HREE + Y anomalies and xenotime ± florencite anomalies. As previously noted, the unconformities and basins were both derived at least in part from the same underlying dataset, and this may be considered a limitation of the model. However, while the HREE + Y anomalies were derived from the NGSA dataset, and the xenotime ± florencite anomalies from the HMMA dataset, and both NGSA and HMMA analyses were performed on the same samples, both were analyzed using independent methods. As such, this is not seen as a limitation of the model, but a positive reinforcement of how different parts of the mineral system interact.

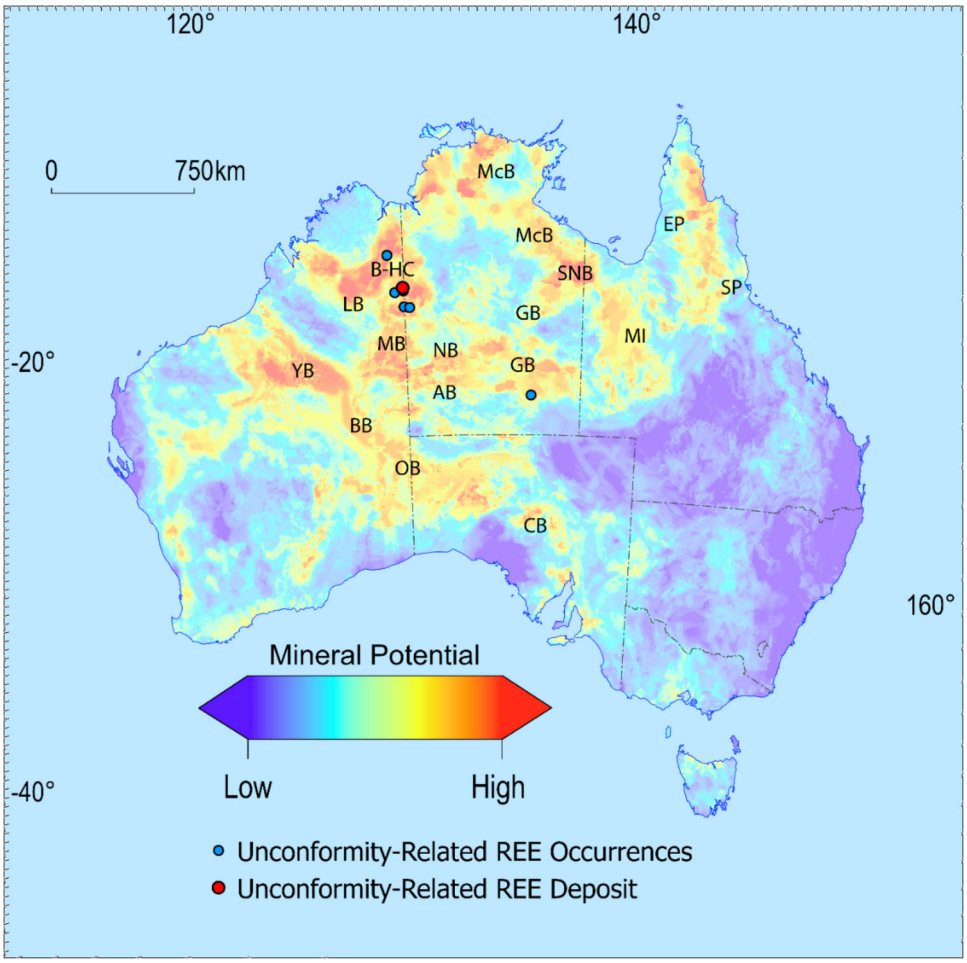

Figure 10. Map showing location of prospective Precambrian basins and provinces. OB–Officer Basin, BB–Bentley Basin, YB–Yeneena Basin, LB–Louisa Basin, B-HC–Birrindudu-Halls Creek region, MB–Murraba Basin, NB–Ngalia Basin, AB–Amadeus Basin, GB–Georgina Basin, SNB–South Nicholson Basin, McB–McArthur Basin, MI–Mount Isa region, EP–Etheridge Province, SP–Savannah Province, CB–Cariewerloo Basin.

In addition, as previously noted, the maps derived from the NGSA and HMMA datasets include a region of missing data across parts of Western Australia and the Northern Territory (Fig. 5b). This region coincides with the location of most of the currently identified URREE deposits and occurrences. While an imputation method was used to infill values in this region (e.g., Ford et al., 2023), the imputed value of 0.5 only considers the binary decision of whether the underlying catchments are prospective or unprospective, and does not accurately reflect the underlying geology. This is likely reflected in the arguably less robust results obtained in the data-driven random forest model, and the lower predictive importance for the input maps derived from these datasets (Fig. 9). The data availability map in Figure 5b highlights the areas where full data coverage is not available and can be viewed in conjunction with the mineral potential maps in Figures 5a, 7a or 8a to provide guidance when assessing the prospective areas for potential follow-up.

It is acknowledged that there are challenges relating to the density of point sample data and depth of cover at the national-scale which affects the use of the NGSA and HMMA datasets. In particular, it was not possible to ascertain which stratigraphic unit or deposit type the geochemical or mineralogical anomalies used to represent parts of the ore deposition component relate to. The

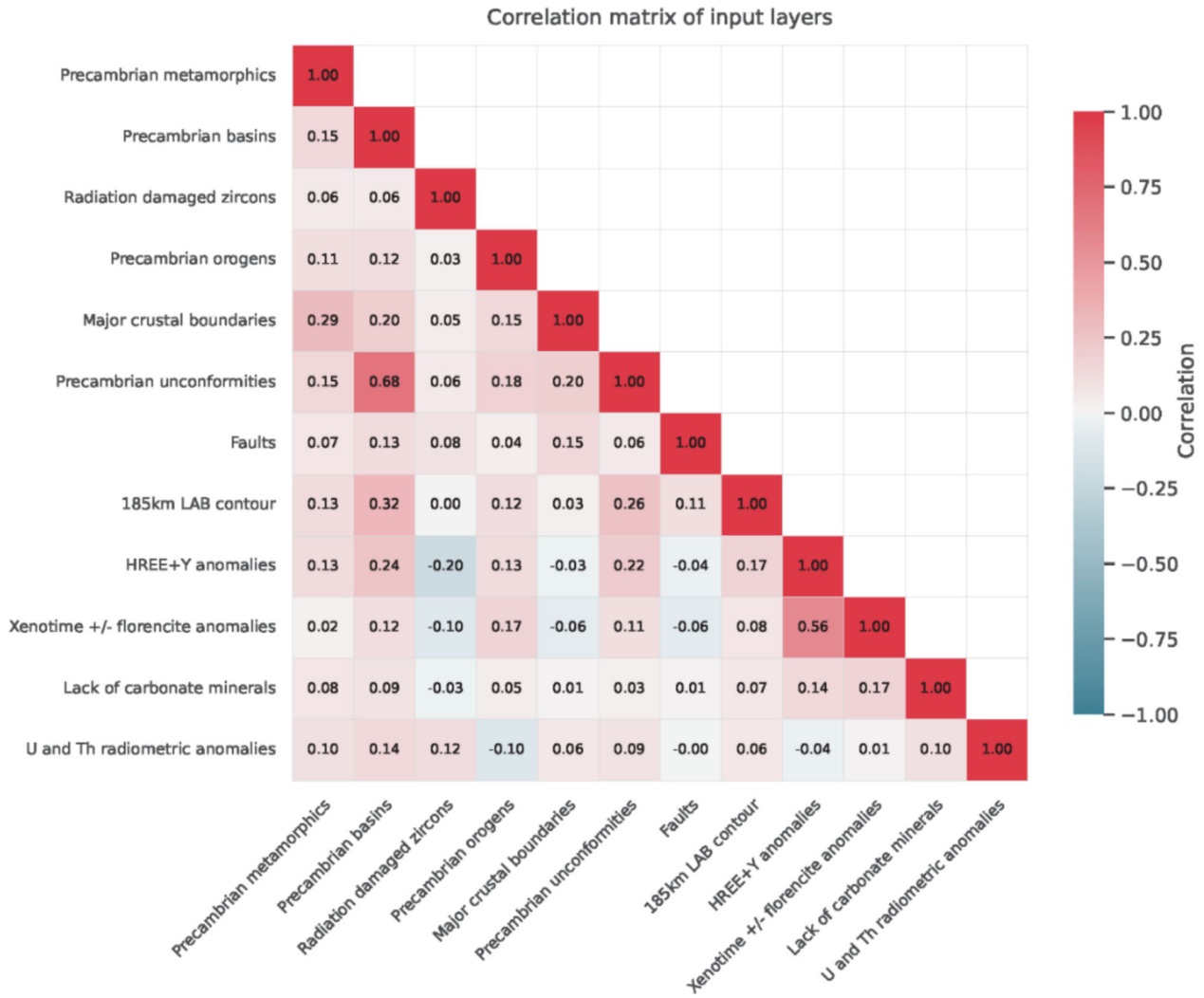

Figure 11. Pairwise correlation matrix for 12 input maps listed in Table 1 highlighting the degree of similarity between the different inputs.

HREE + Y and xenotime ± florencite anomalies could relate to several REE deposit types or stratigraphic units known to be present in Australia, though when combined with other datasets in the model, this issue has limited impact on the model.

While the HMMA dataset was notionally designed to exclude the most common carbonate minerals (e.g., calcite and dolomite), the absolute number of carbonate minerals was not used in the creation of the map of lack of carbonate minerals. The ratio of carbonate mineral grains per sample to the total number of grains in the sample was used. While this may underestimate the absolute value of the ratio, it is expected to have limited impact on the relative values between catchments.

To a lesser extent, the same challenge with the density of point sample data applies to the SHRIMP spot analyses data from which the map of radiation-damaged zircons was derived. Although in this case, while it is clear that national sampling is patchy, it is also noted that even with nominally full national coverage, the sample distribution would still remain biased toward rocks suitable for identifying igneous zircons appropriate for SHRIMP age dating.

Fault data used in the analysis do not discriminate between faults active or inactive at the time of mineralization. Currently, insufficient attribution

exists to consistently query the fault data with this level of granularity and represents an opportunity for further work in the future.

One important caveat when interpreting the model results for exploration targeting is that no depth constraint has been applied in terms of accessibility or economic viability. For example, in areas such as the McArthur Basin, the total thickness in parts of the basin can reach up to 12 km (e.g., Rawlings, 1999). A depth constraint has been left out of the model inputs as it represents an economic or logistical limitation as opposed to geological potential. However, in order to provide a high-level indication of the depth to prospectivity to support decision-making, the 3D chronostratigraphic depth surfaces for the top of Neoarchean (basement), top of Mesoproterozoic, and top of Neoproterozoic were combined and the minimum depth identified for each pixel (Vizy et al., 2024). The minimum depth from this combination of depth surfaces provides an indication of the depth to the top of Precambrian, which is the target age for URREE mineral systems in Australia. Figure 12 shows the modeled depth to top of Precambrian draped over the mineral potential model in Figure 5a. It is noted that these are high-level depth models that do not include detailed stratigraphic depth estimates, and prior to development of detailed exploration targets from the model, geological validation, including more detailed evaluation of basin thickness, should be considered, or targets evaluated through a tool for assessing geospatial economic viability (e.g., Walsh et al., 2020).

The use of a subjective knowledge-driven approach in this mineral potential assessment is due to an insufficient number of currently identified URREE deposits and occurrences available to robustly train and validate a data-driven model. Although a random forest model is presented here for comparison, it is not considered to be reliable due to challenges with the availability of appropriate positive labels, and the majority of known positive labels occurring in an area with limited data coverage. Given a strong focus on exploration for REE in Australia, it is expected that the number of discoveries, including for URREE deposits, will increase over time. As the number of known URREE deposits and occurrences increases, and the underlying data limitations are addressed, it is anticipated that the initial mineral potential models presented in this study could be revised and evaluated using more robust statistical analysis or machine learning techniques to provide an update to the results presented here.

CONCLUSIONS

To support exploration for HREE such as Dy and Tb, a new mineral system model for URREE mineralization in Australia has been presented. Using a knowledge-driven approach, a mineral potential model has been generated using a weighted sum method, which integrates mineral systems expertise and precompetitive geoscience data. The model successfully predicts the location of known URREE deposits and occurrences, reducing the exploration search space by up to 95%. Although a machine learning model was developed and is presented here as a comparison, challenges relating to the amount and spatial distribution of the known deposits and occurrences mean that the random forest model should not be considered robust.

The national-scale mineral potential assessment presented in this study highlights areas with elevated geological potential for URREE mineral systems in Australia. While successfully predicting the location of known URREE mineralization in the Birrindudu–Halls Creek region, demonstrated by high AUC values; high prospectivity areas with no previously identified URREE deposits and occurrences are demonstrated, which may represent new exploration opportunities. This includes parts of the Yeneena, Louisa, Murraba, and South Nicholson basins, which demonstrate both high prospectivity and a relatively shallow depth to Precambrian.

Although challenges relating to data availability and coverage have been noted, novel spatial proxies for key mineral systems processes were mapped and a successful model generated. Additional work on assessing the potential for URREE mineral systems in Australia should focus on the improvement in the underpinning datasets such as the mapped basins, layered geology, faults, NGSA, and HMMA. Updates to these datasets will form part of the 35-year Resourcing Australia's Prosperity initiative at Geoscience Australia. More detailed assessments could also be undertaken at a regional scale, focused on the prospective Precambrian basins in northern Australia.

The mineral potential model produced in this assessment is one of a series of products that will be integrated with national-scale models generated for other REE mineral systems to generate a REE

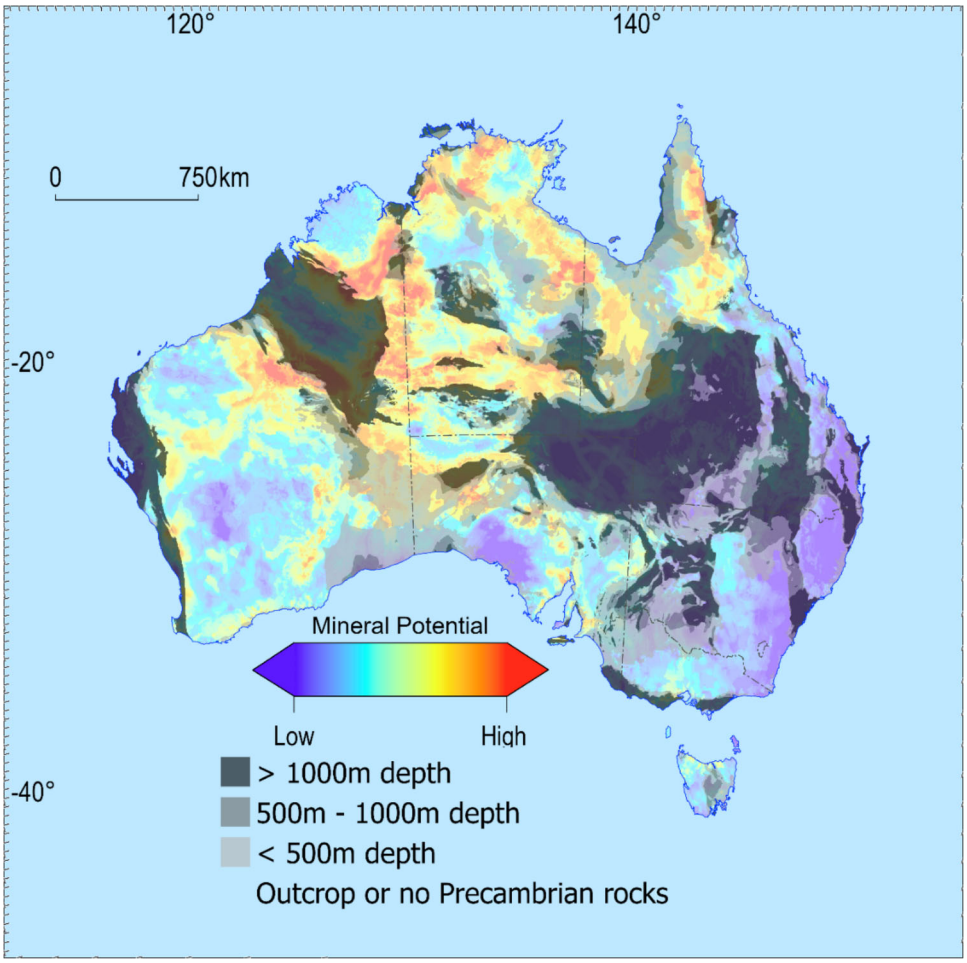

Figure 12. Estimated depth to Precambrian draped over the mineral potential model in Figure 5a. Depth estimates derived from Vizy et al. (2024).

commodity map. These will be consolidated into a REE commodity prospectus with information on other criteria such as re-mining potential, critical mineral by-products, and techno-economics to evaluate Australia's opportunities to supply REEs to the market from both existing and potential new resources.

ACKNOWLEDGMENTS

Geoscience Australia values the lands, water, and sky as we work to deepen a shared understanding of Country and Earth. We respect First Nations Peoples and their enduring connection, contribution, and obligations to Country. Reflecting on our shared history, we are committed to listen and learn. The authors wish to thank colleagues at Geoscience Australia and the state and territory geological surveys for their contributions to the datasets and publications that underpin this assessment. Eloise Beyer and Guillaume Sanchez are thanked for their constructive internal reviews of the manuscript prior to submission. This work was undertaken as part of the Resourcing Australia's Prosperity initiative.

FUNDING

Australian government.

Data AvailabilityReferences to the underpinning data are provided in the Table 1. A data package containing the assessment criteria table and modeling files is available for download from: https://doi.org/10.26186/150681

DECLARATIONS

Conflict of Interest This work was undertaken as part of the Resourcing Australia's Prosperity initiative at Geoscience Australia, which is funded by the Australian government. The authors have no relevant financial or non-financial interests to disclose.

OPEN ACCESS

REFERENCES

Ali, S. H., Giurco, D., Arndt, N., Nickless, E., Brown, G., Demetriades, A., Durrheim, R., Enriquez, M. A., Kinnaird, J., Littleboy, A., & Meinert, L. D. (2017). Mineral supply for sustainable development requires resource governance. *Nature, 543*, 367–372.

Beard, C. D., Goodenough, K. M., Borst, A. M., Wall, F., Siegfried, P. R., Deady, E. A., Pohl, C., Hutchison, W., Finch, A. A., Walter, B. F., & Elliott, H. A. (2023). Alkaline-silicate REE-HFSE systems. *Economic Geology, 118*, 177–208.

Bruce, M., Kreuzer, O., Wilde, A., Buckingham, A., Butera, K., & Bierlein, F. (2020). Unconformity-type uranium systems: A comparative review and predictive modelling of critical genetic factors. *Minerals, 10*, 738.

de Caritat, P., & Cooper, M. (2011). *National geochemical survey of Australia: the geochemical atlas of Australia: Dataset*. Geoscience Australia. https://doi.org/10.11636/Record.2011.020.

Choi, W., Pyun, S., & Jou, H.-T. (2025). Synthetic training data optimization for enhanced fault detection in seismic images. *Lithosphere, 2025*, lithosphere_2024_240.

Colquhoun, G.P., Hughes, K.S., Deyssing, L., Ballard, J.C., Folkes, C.B., Phillips, G., Troedson, A.L. and Fitzherbert, J.A. (2025). New South Wales seamless geology dataset, version 2.5 [Digital Dataset]. Geological Survey of New South Wales, Department of Primary Industries and Regional Development, Maitland. https://search.geoscience.nsw.gov.au/product/9266.

Critical Minerals Office. (2024). Australia's critical minerals list and strategic materials list. https://www.industry.gov.au/publications/australias-critical-minerals-list-and-strategic-materials-list. [accessed 30/10/2025].

Czarnota, K., Hoggard, M. J., Richards, F. D., Teh, M., Huston, D. L., Jaques, A. L., & Ghelichkhan, S. (2020). Minerals on the edge: sediment-hosted base metal endowment above steps in lithospheric thickness. In K. Czarnota, I. Roach, S. Abbott, M. Haynes, N. Kositcin, A. Ray, & E. Slatter (Eds.), *Exploring for the future: Extended abstracts* (pp. 1–4). Geoscience Australia. https://doi.org/10.11636/134991.

Department of Primary Industry and Resources. (2025). Northern Territory Geological Survey–mineral occurrence database (MODAT). https://geoscience.nt.gov.au/gemis/ntgsjspui/handle/1/81745. [accessed 30/06/2025].

Department of Mines, Industry Regulation and Safety. (2025). MINEDEX database. http://www.dmp.wa.gov.au/datacentre. [accessed 30/06/2025].

Department of Natural Resources and Mines, Manufacturing, and Regional and Rural development. (2025). Detailed geology structure–Queensland. Geological Survey of Queensland. [accessed 20/08/2025].

Department of Energy, Environment and Climate Action. (2025). Shear displacement structures (1:250,000). Geological Survey of Victoria. https://discover.data.vic.gov.au/dataset/shear-displacement-structures-1-250000. [accessed 20/08/2025].

Doublier, M. P., & Korsch, R. J. (2024). *Major crustal boundaries of Australia* (2024th ed.). Geoscience Australia. https://doi.org/10.26186/149663.

Ewing, R. C., Meldrum, A., Wang, L., Weber, W. J., & Corrales, L. R. (2003). Radiation effects in zircon. *Reviews in Mineralogy and geochemistry, 53*, 387–425.

Ford, A., Huston, D., Cloutier, J., Doublier, M., Schofield, A., Cheng, Y., & Beyer, E. (2023). A national-scale mineral potential assessment for carbonatite-related rare earth element mineral systems in Australia. *Ore Geology Reviews, 161*, Article 105658.

Ford, A., Peters, K. J., Partington, G. A., Blevin, P. L., Downes, P. M., Fitzherbert, J. A., & Greenfield, J. E. (2019). Translating expressions of intrusion-related mineral systems into mappable spatial proxies for mineral potential mapping: Case studies from the Southern New England Orogen, Australia. *Ore Geology Reviews, 111*, Article 102943.

Geological Survey of Western Australia. (2022). 1:500 000 tectonic units of Western Australia, November 2022 update. http://www.dmp.wa.gov.au/geoview [accessed 18/08/2025].

Geological Survey of Western Australia. (2025). 1:500 000 Interpreted bedrock geology of Western Australia. Geological Survey of Western Australia. https://catalogue.data.wa.gov.au/dataset/1-500-000-state-interpreted-bedrock-geology-dmirs-016 [accessed 20/08/2025].

Geological Survey of South Australia. (2025a). Solid geology: Archaean–early mesoproterozoic faults. Geological Survey of South Australia. https://pid.sarig.sa.gov.au/dataset/mesac656 [accessed 20/08/2025].

Geological Survey of South Australia. (2025b). Solid geology: Middle mesoproterozoic faults. Geological Survey of South Australia. https://pid.sarig.sa.gov.au/dataset/mesac71 [accessed 20/08/2025].

Geological Survey of South Australia. (2025c). Solid geology: Late mesoproterozoic faults. Geological Survey of South Australia. https://pid.sarig.sa.gov.au/dataset/mesac759 [accessed 20/08/2025].

Geological Survey of South Australia. (2025d). Solid geology: Neoproterozoic–ordovician faults. Geological Survey of South Australia. https://pid.sarig.sa.gov.au/dataset/mesac581 [accessed 20/08/2025].

Geoscience Australia. (2025). Sensitive high resolution ion microprobe (SHRIMP)—analyses. Geoscience Australia, Canberra. https://portal.ga.gov.au/metadata/33d9d8e7-f310-43d5-b50a-7fbdd03cab43 [accessed 01/07/2025].

Geoscience Australia and Australian Stratigraphy Commission. (2025). Australian stratigraphic units database. https://asud.ga.gov.au/ [accessed 01/07/2025].

Goodenough, K. M., Wall, F., & Merriman, D. (2018). The rare earth elements: Demand, global resources, and challenges for resourcing future generations. *Natural Resources Research, 27*, 201–216.

Gysi, A. P., Williams-Jones, A. E., & Harlov, D. (2015). The solubility of xenotime-(Y) and other HREE phosphates ($DyPO_4$, $ErPO_4$ and $YbPO_4$) in aqueous solutions from 100 to 250 °C and p_{sat}. *Chemical Geology, 401*, 83–95.

Hoggard, M. J., Czarnota, K., Richards, F. D., Huston, D. L., Jaques, A. L., & Ghelichkhan, S. (2020). Global distribution of sediment-hosted metals controlled by craton edge stability. *Nature Geoscience, 13*, 504–510.

Huston, D., Cloutier, J., Burnham, A., Cheng, Y., Doublier, M., & Downes, P. M. (2024). *Geological setting, age and endowment of major Australian mineral deposits–a compilation (2024 update)*. Geoscience Australia. https://doi.org/10.26186/149917.

Huston, D. (2024). Global rare earth element deposits–a compilation. GA Record 2024/03. Geoscience Australia, Canberra. https://doi.org/10.26186/148953.

International Energy Agency. (2025). Global critical minerals outlook 2025, IEA, Paris https://www.iea.org/reports/global-critical-minerals-outlook-2025, [accessed 30/10/2025].

Jaireth, S., Hoatson, D. M., & Miezitis, Y. (2014). Geological setting and resources of the major rare-earth-element deposits in Australia. *Ore Geology Reviews, 62*, 72–128.

Lawley, C. J. M., McCafferty, A. E., Graham, G. E., Huston, D. L., Kelley, K. D., Czarnota, K., Paradis, S., Peter, J. M., Hayward, N., Barlow, M., Emsbo, P., Coyan, J., San Juan, C. A., & Gadd, M. G. (2022). Data–driven prospectivity modelling of sediment–hosted Zn–Pb mineral systems and their critical raw materials. *Ore Geology Reviews, 141*, Article 104635.

Liu, S.-L., Fan, H.-R., Liu, X., Meng, J., Butcher, A. R., Yann, L., Yang, K.-F., & Li, X.-C. (2023). Global rare earth elements projects: New developments and supply chains. *Ore Geology Reviews, 157*, Article 105428.

Magee, C.W., Nasdala, L., Dubosq, R., Gault, B., and Bodorkos, S. (2025). Technical note: Investigation into the mechanism of chemical abrasion using SHRIMP, Raman spectroscopy and atom probe tomography. EGUsphere [preprint], https://doi.org/10.5194/egusphere-2025-1810.

Meyer, M., & Brooker, J. (1991). *Eliciting and analysing expert judgement: A practical guide*. Academic Press.

Migdisov, A., Williams-Jones, A. E., Brugger, J., & Caporuscio, F. A. (2016). Hydrothermal transport, deposition, and fractionation of the REE: Experimental data and thermodynamic calculations. *Chemical Geology, 439*, 13–42.

Mineral Resources Tasmania. (2025). 1:250,000 geology data and maps. Mineral Resources Tasmania. https://www.mrt.tas.gov.au/products/digital_data/data_downloads/geology_of_tasmania [accessed 20/08/2025].

Morin-Ka, S., Beardsmore, T.J., Hancock, E.A., Rasmussen, B., Dunkley, D., Zi, J., Muhling, J., Wilson, R., & Chapman, J. (2016). Alteration and age of the Browns Range heavy rare earth element deposits. In: GSWA 2016 Extended Abstracts: Promoting the Prospectivity of Western Australia: Geological Survey of Western Australia Record, 2 (2016), 21–25.

Nazari-Dehkordi, T., Huizenga, J. M., Spandler, C., & Oliver, N. H. (2019). Fluid inclusion and stable isotope constraints on the heavy rare earth element mineralisation in the Browns Range Dome, Tanami Region. *Western Australia. Ore Geology Reviews, 113*, Article 103068.

Nazari-Dehkordi, T., & Spandler, C. (2019). Paragenesis and composition of xenotime-(Y) and florencite-(Ce) from unconformity-related heavy rare earth element mineralization of northern Western Australia. *Mineralogy and Petrology, 113*, 563–581.

Nazari-Dehkordi, T., Spandler, C., Oliver, N. H. S., Chapman, J., & Wilson, R. (2017). Provenance, tectonic setting and source of Archean metasedimentary rocks of the Browns Range Metamorphics, Tanami Region, Western Australia. *Australian Journal of Earth Sciences, 64*, 723–741.

Nazari-Dehkordi, T., Spandler, C., Oliver, N. H., & Wilson, R. (2018). Unconformity-related rare earth element deposits: a regional-scale hydrothermal mineralization type of Northern Australia. *Economic Geology, 113*, 1297–1305.

Nazari-Dehkordi, T., Spandler, C., Oliver, N. H., & Wilson, R. (2020). Age, geological setting, and paragenesis of heavy rare earth element mineralization of the Tanami region, Western Australia. *Mineralium Deposita, 55*, 107–130.

Northern Minerals Limited. (2025). ASX announcement 16 January 2025. https://yourir.info/resources/f912a5b0cde73f4b/announcements/ntu.asx/6A1247151/NTU_2025_Wolverine_Mineral_Resource_Estimate.pdf [accessed 18/02/2026].

Northern Territory Geological Survey and Geognostics Australia Pty Ltd. (2021). Northern Territory SEEBASE® and GIS. Northern Territory Geological Survey, Digital Information Package DIP 030. https://geoscience.nt.gov.au/gemis/ntgsjspui/handle/1/91172.

Northern Territory Geological Survey. (2023). Northern Territory geological faults 2500K. Northern Territory Geological Survey. https://data.nt.gov.au/dataset/strike—northern-territory-geological-faults-2500k. [accessed 20/08/2025].

Nykänen, V., Törmänen, T., & Niiranen, T. (2023). Cobalt prospectivity using a conceptual fuzzy logic overlay method enhanced with the mineral systems approach. *Natural Resources Research, 32*, 2387–2416.

Parsa, M., & Cumani, R. (2025). Class label representativeness in machine learning-based mineral prospectivity mapping. *Natural Resources Research, 34*, 1901–1925.

Parsa, M., Lawley, C. J. M., Cumani, R., Schetselaar, E., Harris, J., Lentz, D. R., Zhang, S. E., & Bourdeau, J. E. (2024). Predictive modeling of Canadian carbonatite-hosted REE +/− Nb deposits. *Natural Resources Research, 33*, 1941–1965.

Rabiei, M., Chi, G., Normand, C., Davis, W. J., Fayek, M., & Blamey, N. J. F. (2017). Hydrothermal rare earth element (xenotime) mineralization at Maw Zone, Athabasca Basin, Canada, and its relationship to unconformity-related uranium deposits. *Economic Geology, 112*, 1483–1507.

Rawlings, D. J. (1999). Stratigraphic resolution of a multiphase intracratonic basin system: The McArthur Basin, northern Australia. *Australian Journal of Earth Sciences, 46*, 703–723.

Raymond, O. L. (2018). *Australian geological provinces* (2018.01). Geoscience Australia. https://doi.org/10.26186/116823.

Raymond, O. L., Liu, S., Gallagher, R., Zhang, W., & Highet, L. M. (2012). *Surface geology of Australia 1:1 million scale dataset* (2012th ed.). Geoscience Australia. https://doi.org/10.26186/74619.

Rodriguez-Galiano, V. F., Chica-Olmo, M., & Chica-Rivas, M. (2014). Predictive modelling of gold potential with the integration of multisource information based on random forest: a case study on the Rodalquilar area. *Southern Spain: Inter-*

national Journal of Geographical Information Science, 28, 1336–1354.

Sanchez, G., Stewart, A. J., Liu, S. F., Highet, L., Woods, M., Brown, C., Bonnardot, M., Beyer, E., Clark, A., Connors, K., Wong, S., Cayley, R., Skladzien, P., Czarnota, K., Buddee, M., MaraisvanVuuren, C., Cassells, L., Oborski, E., Knepprath, N., … Werner, M. (2024). *Layered Geology of Australia, 1:1 000 000 scale dataset* (2024th ed.). Geoscience Australia. https://doi.org/10.26186/149179.

Skirrow, R. G., Murr, J., Schofield, A., Huston, D. L., van der Wielen, S., Czarnota, K., Coghlan, R., Highet, L. M., Connolly, D., Doublier, M., & Duan, J. (2019). Mapping iron oxide Cu-Au (IOCG) mineral potential in Australia using a knowledge-driven mineral systems-based approach. *Ore Geology Reviews, 113*, Article 103011.

Spandler, C., Slezak, P., & Nazari-Dehkordi, T. (2020). Tectonic significance of Australian rare earth element deposits. *Earth Science Reviews, 207*, Article 103219.

Sudholz, Z. J., Jaques, A. L., Yaxley, G. M., Taylor, W. R., Czarnota, K., Haynes, M. W., Frewer, L., Ramsay, R. R., Downes, P. J., & Cooper, S. A. (2023). Mapping the structure and metasomatic enrichment of the lithospheric mantle beneath the Kimberley Craton, Western Australia. *Geochemistry, Geophysics, Geosystems, 24*, e2023GC011040.

Valetich, M., Zivak, D., Spandler, C., Degeling, H., & Grigorescu, M. (2022). REE enrichment of phosphorites: An example of the Cambrian Georgina Basin of Australia. *Chemical Geology, 588*, Article 120654.

Vizy, J., Rollet, N., & Nicoll, M. (2024). *Preliminary 3D chronostratigraphic model of australia–data package of 3D modelling chronostratigraphic surfaces and isochores, Version 1.0*. Geoscience Australia. https://doi.org/10.26186/149923.

Walsh, S. D. C., Northey, S. A., Huston, D., Yellishetty, M., & Czarnota, K. (2020). Bluecap: A geospatial model to assess regional economic-viability for mineral resource development. *Resources Policy, 66*, Article 101598.

Walsh, J. M. J., & Spandler, C. (2023). The role of zircon in hydrothermal heavy REE mineralisation: The case for unconformity-related ore deposits of north-west Australia. *Chemical Geology, 629*, Article 121493.

Weng, Z., Jowitt, S. M., Mudd, G. M., & Haque, N. (2015). A detailed assessment of global rare earth element resources: opportunities and challenges. *Economic Geology, 110*, 1925–1952.

Whelan, J., McGloin, M., Close, D., Maas, R., Walsh, J., and Spandler, C. (2023). Demystifying the Arthur Pope's prospect: REE, Y and Cu bearing carbonate-quartz veins in the Casey Inlier, central Australia, Northern Territory Geological Survey Annual Geoscience Exploration Seminar (AGES) 2023: Alice Springs, Northern Territory Geological Survey.

Wilford, J.R. and Kroll, A. (2020). Complete radiometric grid of Australia (Radmap) v4 2019 with modelled infill. Geoscience Australia, Canberra. https://pid.geoscience.gov.au/dataset/ga/144413.

Yin, J. N., & Song, X. (2022). A review of major rare earth element and yttrium deposits in China. *Australian Journal of Earth Sciences, 69*, 1–25.

de Caritat, P., Walker, A.T., Bastrakov, E., Main, P., & McInnes, B.I.A. (2023). The heavy mineral map of Australia project. Final data release: National dataset and atlas. Geoscience Australia, Canberra. https://doi.org/10.26186/148916.